EUROFUSION WPS2-PR(16) 14914

FM Castejon et al.

Influence of magnetic well on electromagnetic turbulence in the TJ-II stellarator

Preprint of Paper to be submitted for publication in
Plasma Physics and Controlled Fusion

This work has been carried out within the framework of the EUROfusion Consortium and has received funding from the Euratom research and training programme 2014-2018 under grant agreement No 633053. The views and opinions expressed herein do not necessarily reflect those of the European Commission.

Influence of magnetic well on electromagnetic turbulence in the TJ-II stellarator

F. Castejón, A. M. Aguilera, E. Ascasíbar, T. Estrada, C. Hidalgo, A. López-Fraguas, M. A. Ochando, S. Yamamoto[a], A.V. Melnikov[b,c], L.G. Eliseev[b], S.V. Perfilov[b], and the TJ-II Team

Laboratorio Nacional de fusión. CIEMAT. Av Complutense 22. 28040 Madrid. Spain

[a]Institute of Advanced Energy, Kyoto University, Uji, Japan

[b]National Research Centre, NRC 'Kurchatov Institute', 123182, Moscow, Russia

[c]National Research Nuclear University MEPhI, Moscow, Russia

Abstract

Magnetic well scan has been performed in TJ-II to investigate the confinement properties with different values of the well, or even of the hill, and to explore the properties of electromagnetic turbulence. Stable plasmas have been obtained in theoretically Mercier-unstable configurations, and the electrostatic turbulence levels in the edge are increased. Three families of modes appear during the experiments: 1) a family of modes of Alfvénic nature with high frequencies; 2) a second set of modes of middle frequencies (tens of kHz) and 3) an oscillation at $f \approx$10-20 KHz happens in several cases. In spite of the fact that the vacuum rotational transform is very similar in all the cases, the Alfvénic mode family changes drastically when decreasing the magnetic well, showing a non-monotonic behaviour of the amplitude, and a decrease of the typical frequencies. This behaviour cannot be explained either considering current or density variations, so it must be attributed to the modification of the configuration. Regarding the intermediate frequencies, a coherent mode appears with decreasing frequency as the magnetic well decreases. This mode is assumed to be a GAM, which can survive in these TJ-II plasmas, despite of the strong damping.

1.- Introduction.

Magnetic well is a key ingredient to stabilise interchange modes in stellarators and, hence, is taken into account when performing stellarator optimization, neoclassical transport and stability (see e. g. [1]). Mercier criterion provides stability against interchange modes and is usually considered among the optimization criteria[2]. The Mercier criterion is obtained from the energy functional with respect to the displacement localised in a given magnetic surface [[3]], giving the local stellarator stability. Making positive the second functional derivative of the energy functional against radially localised perturbations provides a guide to elucidate the linear stability of a 3D complex magnetic configuration. The inequality implies that (see [[4]] and references therein):

$$D_M(\rho) = D_W(\rho) + D_S(\rho) + D_I(\rho) + D_{\mathrm{K}}(\rho) \geq 0 \qquad (1)$$

The first term of the rhs represents the stabilising contribution of the magnetic well, the second one corresponds to the magnetic shear, which is stabilising, the third one corresponds to the plasma current, which can stabilise or destabilise [[5]], depending on its sign and on the possible introduction of resonances in the plasma column. The last one comes from the geodesic curvature, which presents stable or unstable zones of the plasma, depending on its relative sign with the pressure gradient. Therefore, it is seen the magnetic well, related to shape of magnetic surfaces, is a key stabilizing ingredient and, hence, the optimized configurations are usually complex and must be created by complicated coils, difficult to build and to maintain, which is especially relevant for a stellarator-based reactor, where the operations of maintenance must be performed using remote handling techniques. Therefore the relaxing of such a criterion can help to design simpler and cheaper stellarators.

The flexible heliac TJ-II[6] is an almost shearless device and its plasma current is very small, therefore the Mercier stability is a competition between the magnetic well and the geodesic curvature. These two quantities are related and the deeper well is accompanied by less destabilising curvature. TJ-II allows one to vary the magnetic well, keeping constant the rotational transform profile, although the volume values of the magnetic configurations are reduced as the magnetic well decreases, making it possible to explore the turbulence and confinement properties of this device for different values of the well.

Figure 1 shows the magnetic well and the rotational transform profiles and the volume values for the family of configurations used for these experiments. Figure 2 shows the Poincaré plots of the field lines of magnetic surfaces of three configurations, the ones with largest and least magnetic well and an intermediate configuration. It is also possible to see the islands corresponding to n/m=8/5 resonance at $\rho \approx 0.8$.

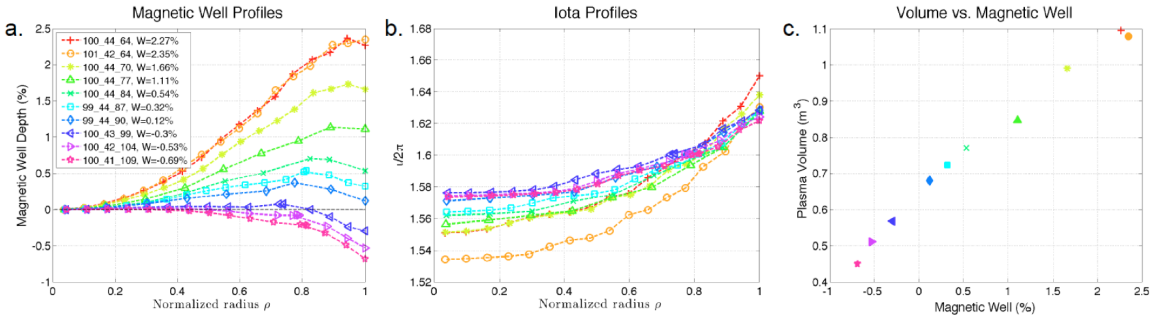

Figure 1: a) Profiles of magnetic well of the family of TJ-II configurations used for these experiments; b) rotational transform profiles and c) volumes of these configurations.

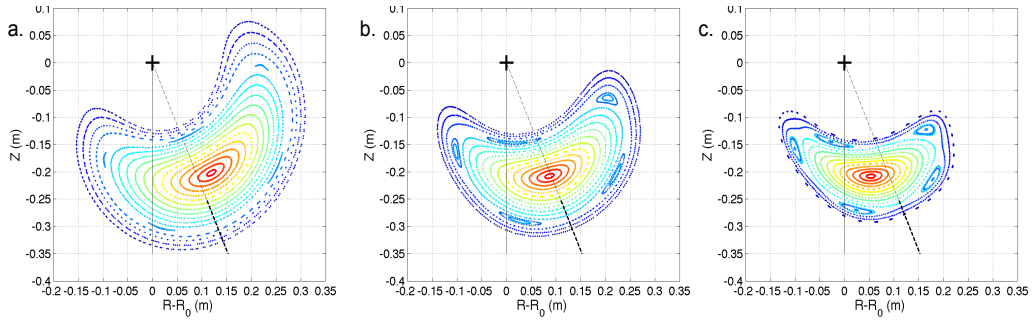

Figure 2: Poincaré plots corresponding to: a) the configuration with largest magnetic well W=2.36 %; b) an intermediate configuration with W=0.32 %; c) the configuration with largest hill W=-0.69 %.

These magnetic well scan experiments on TJ-II have shown the existence of stable plasmas in Mercier-unstable magnetic configurations[7]. Figure 3 (taken from Reference [7]) shows the energy confinement time of the plasmas in this family of configurations, showing that the degradation that happens for configurations with magnetic hill is due to the decreasing plasma volume rather than to the configuration itself. The position of the last closed magnetic surface (LCFS) is the same as the predicted by the VMEC[8] equilibrium

calculations in all the cases, despite the presence of the n/m=8/5 rational at effective radius $\rho \approx 0.8$.

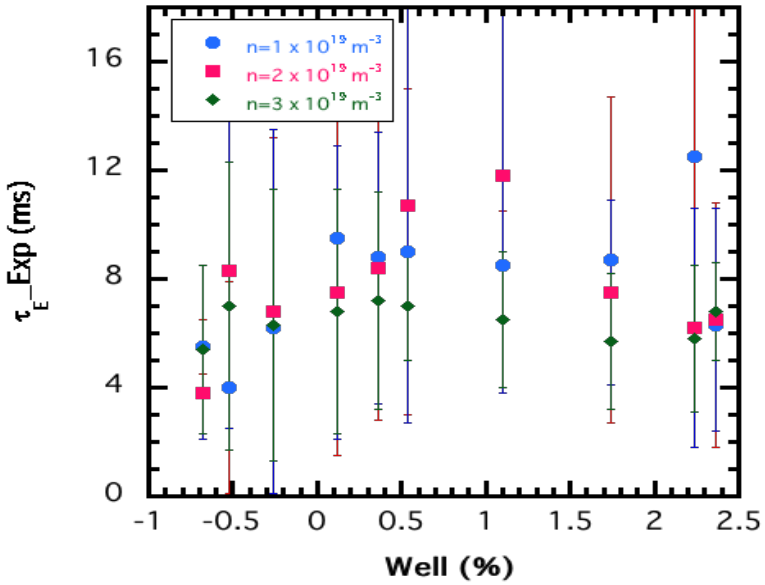

Figure 3: Confinement time for three densities as a function of the magnetic well.

In this work, we explore the electromagnetic properties of the turbulence during the magnetic well scan. The reminder of the paper is organised as follows: section 2 is devoted to the experimental set-up; section 3 shows…

2.- Experimental set-up and results.

The plasmas of these experiments were created and heated by two gyrotrons that launch 250 kW of power each, at X mode with frequency f=53.2 GHz. The two neutral beam injectors (NBI) can launch up to 600 kW each. One of the injectors launch fast neutral co-directed to the magnetic field, while the other performs counter-injection with respect to the magnetic field.

The experimental set-up consists of Langmuir Probes, Mirnov coils, Heavy Ion Bem Probe, arrays of bolometers and a Doppler reflectometer. Langmuir probes are able to measure floating potential in the very edge of the plasma and they have shown that the level of electrostatic turbulence shows an increase as the magnetic well decreases and becomes magnetic hill [7], although it has small effects of confinement, if any. The rms of the fluctuations of the electrostatic potential is used there to characterise the turbulence level.

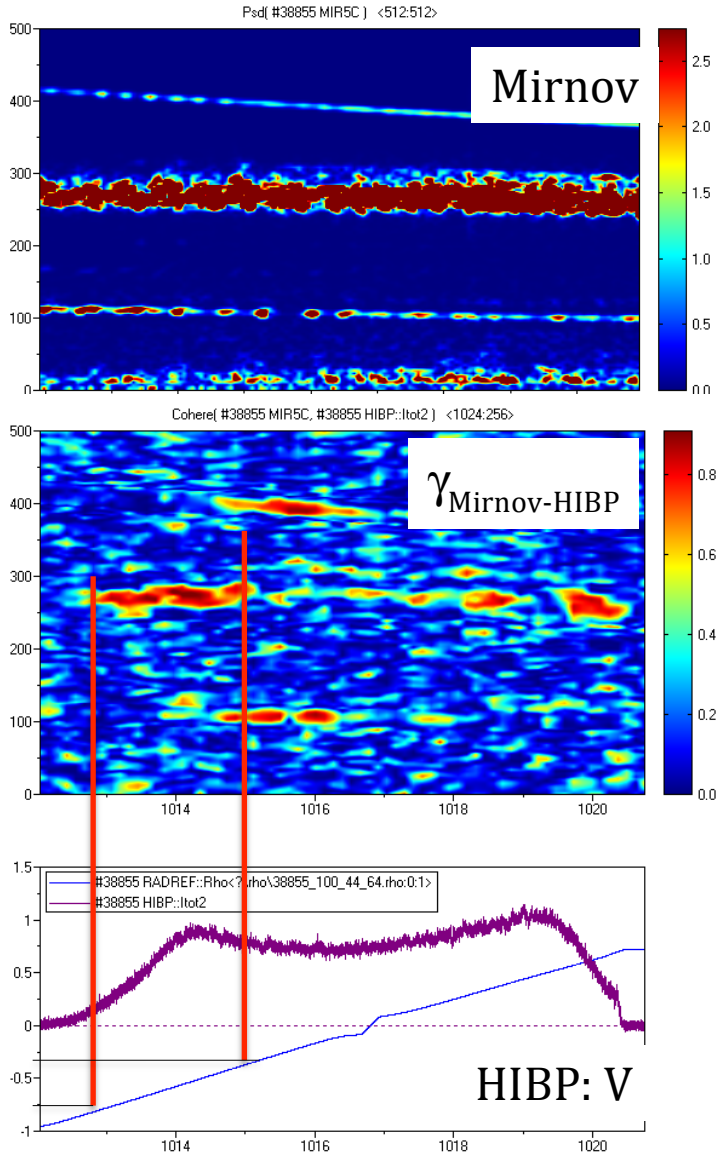

Figure 4: Time evolution of the Mirnov coil signal spectrogram (Top); coherence between Mirnbov coil and HIBP signals (Middle) and electrostatic potential measured by HIBP and effective radius of the measurement, positive means LFS and negative HFS (Bottom).

Mirnov coils can detect magnetic fluctuations in the outer part of the plasma (typically $\rho \geq 0.4$), and this diagnostic can be used to detect the position of the mode in combination with HIBP[9], which can measure the electrostatic potential and its fluctuations along the whole radius in some of the configurations. The mode is localised radially by scanning the measurement position of the HIBP along the minor radius and calculating the coherence between the HIBP and the Mirnov coil signals. The maximum will indicate the position of the mode. Figure 4 shows the time evolution of the spectrogram of the Mirnov coil signal (top panel) together with the electrostatic potential measured by HIBP and the corresponding radial position (shown at the bottom panel, where negative radius means high field side and positive one means low field side). The coherence of these two signals shows the location of the mode, since it is located at the radial positions where the coherence is maximum (middle panel). In this particular case the mode is located at the radial positions $0.65 \geq \rho \geq 0.4$, in the high field side.

2.1- Spatial structure of the turbulence.

The broadband turbulence is measured by Doppler reflectometer [10] on this configuration scan at the interval $0.7 < \rho < 0.85$. A set of reproducible discharges in the same configuration with a given scan is performed to probe the turbulence level at different perpendicular wave vector at a given position (see Figure 5, where the probed wave vector for the magnetic configurations are plotted). The turbulence level is, therefore, obtained at the radial positions where the wave is reflected and for the chosen wave vectors in plasmas with different magnetic wells. Figure 6 shows the turbulence level for the same positions, wave vectors and configurations of Figure 5, conserving the colour code. Finally, all the points are plotted together in Figure 7, showing a single spectrum of perpendicular wave vector for all the cases. This means that the wave vector spectrum is the same, for the same values of densities, in all the cases. Therefore, the spatial structure of the turbulence is the same for those cases.

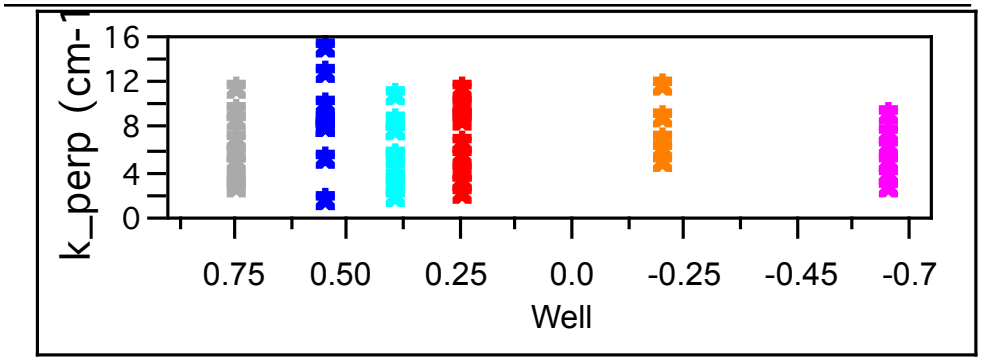

Figure 5: Wave vectors explored by the Doppler reflectometer at configurations with different values of the magnetic well.

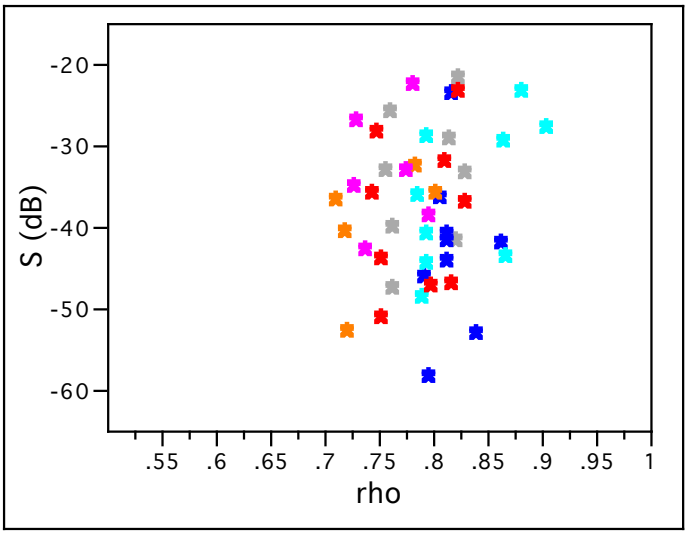

Figure 6: Turbulence level at different radial positions and magnetic configurations, measured by the Doppler reflectometer, with the same colour code of figure 5.

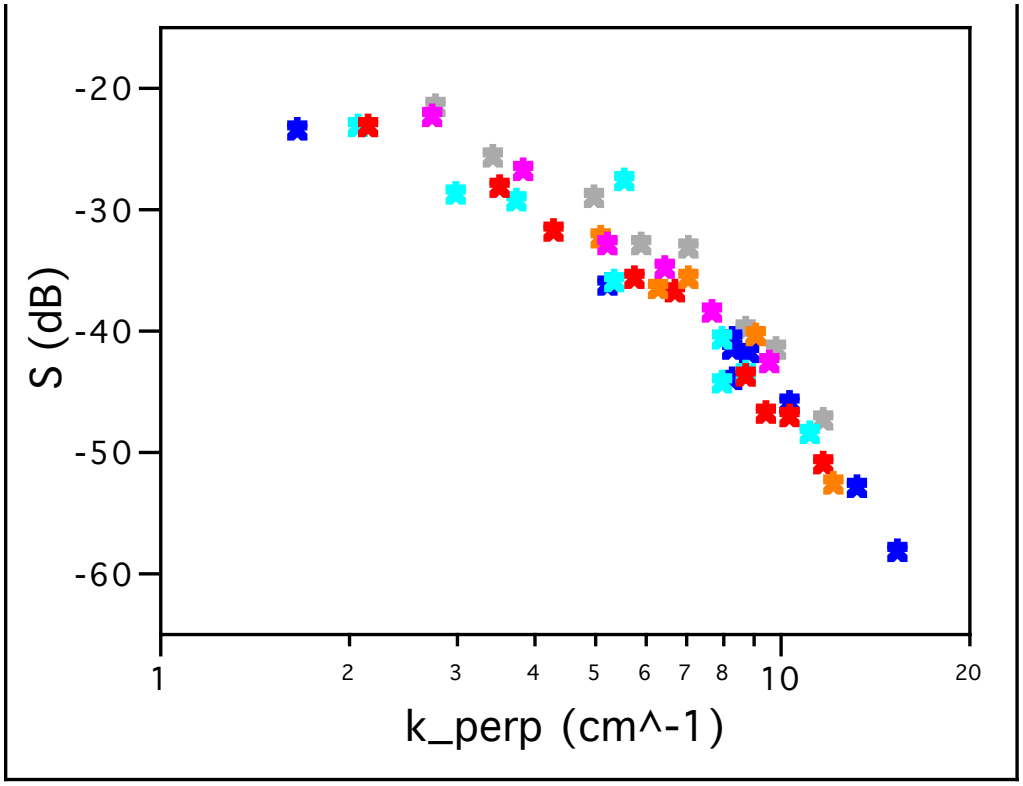

Figure 7: Spectrum of wave vector for all the configurations and positions.

2.2 Coherent mode spectra

The spectra of the signal measured by the Langmuir probe at different magnetic configurations are obtained and plotted in Figure 8 for NBI co-injection. It is seen that, for frequencies larger than several tens of KHz, a coherent mode appears with frequencies lower and lower as magnetic well decreases. The cause for the variation of the frequency cannot be attributed either to the density or the current, as we will show below. The Alfvén frequency is given by:

$$2\pi f = k_{\parallel} v_A \approx \frac{B}{\left(M\mu_0\right)^{1/2}\sqrt{n_e}}\left|m\iota - n\right| \qquad (2)$$

In this expression n_e is the electron density, M is the average ion mass, m and n are the poloidal and toroidal numbers of the mode. In these shots of TJ-II, it is possible to estimate the change of iota from the vacuum iota value by a simple formula [11]:

$$\iota(\rho) = \iota_{vac}(\rho) + C(\rho) I_p \qquad (3)$$

Where I_p is the plasma current, and $C(\rho)$ is a weakly depending function of effective radius. The variation of the Alfvén frequency varies as:

$$2\pi f = \frac{B}{\left(M\mu_0\right)^{1/2}\sqrt{n_e}}\left|m(C\left(\rho\right) I_p + \iota_{vac}) - n\right| \sim \pm\frac{\left|I_p\right|}{\sqrt{n}} \qquad (4)$$

In fact, it is possible to see how the frequency evolving following the former expression (see Figure 10). Then, the changes in density and current for the configuration scan we are dealing with cannot explain the reduction of the frequency.

It could be also possible that the change of frequency is due to the modification of fast particle population. Nevertheless, experiments with counter-injection, with a different fast ion population [12], show the same trend, which implies that the responsible for this trend is the configuration change.

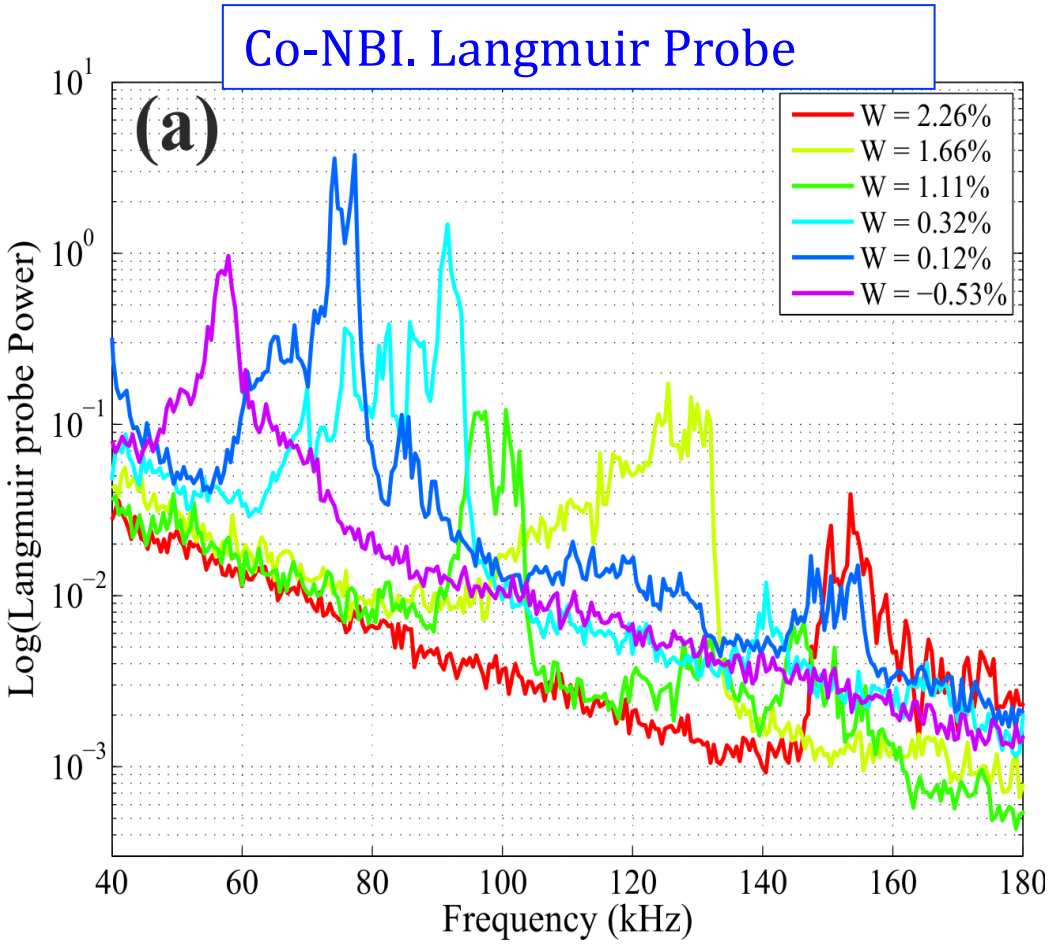

Figure 8: Spectra of coherent modes measured by Langmuir probes for the configurations with different magnetic well values.

3.- Characterization of the modes.

3.1. Low frequencies (up to 20 kHz)

The family of configurations in this magnetic well scan is characterised for having the resonance 8/5 at $\rho \approx 0.8$ in vacuum. The onset of an oscillation at f≈10 - 20 KHz happens in several cases, showing that the mode creates a rotating island (see [13] for the effect of a rotating island) mainly in configurations with low magnetic well or magnetic hill, although this behaviour is not systematic. The behaviour of the island depends strongly on plasma current, which is able to move the resonance outwards in the plasma, when it takes negative values, or to inner positions for $I_p > 0$. The change of the position of resonance with respect to vacuum is given by $\rho \approx 0.1\ I_p$(kA). The onset of the island could have influence on the Alfvénic spectrum[14], since the structure of magnetic field is modified.

3.2 Intermediate frequencies: Global Acoustic Modes

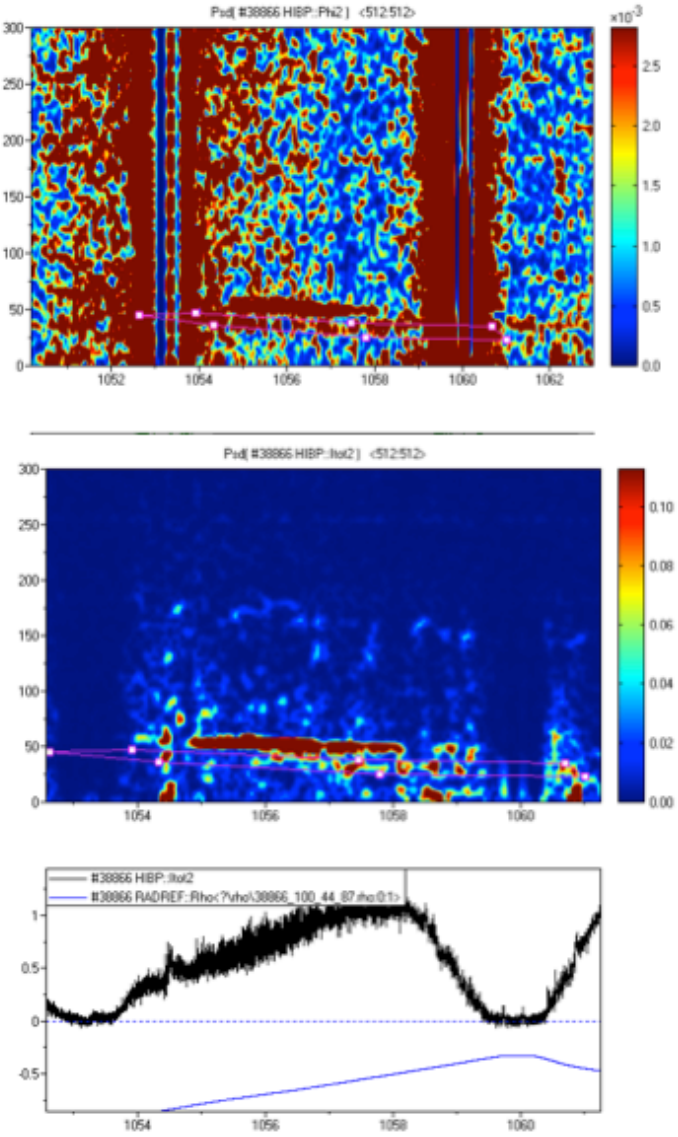

Figure 9: Time evolution of the HIBP signals. Top panel: spectrogram of density; middle panel: spectrogram of potential; bootom panel: electrostatic potential measured and effective radius of the measurement. In this case only HFS can be accessed by HIBP.

In the case of counter-NBI a mode appears in the configurations with intermediate magnetic well. This mode appears at frequencies close to f = 50 kHz. Figure 9 shows the characteristics of this mode in the configuration 100_44_87, with middle magnetic well W = 0.32 %, measured with HIBP. It is seen that the mode is more pronounced in potential than in density, which are the characteristics of global acoustic modes (GAM) of electromagnetic nature. The location of the mode is around $\rho \approx 0.5$, in the HFS, with a width $\rho \approx 0.2$, as can be seen in the bottom panel of the figure. In this case, the HIBP is only capable of sweeping the HFS of the plasma, because of the shape of this configuration.

The linear gyrokinetic calculations on TJ-II show that a GAM appears at frequencies f = 50 kHz [[15]]. Nevertheless, those calculations also predict a strong collisionless damping of this type of modes in the high ripple TJ-II configurations, which should prevent their appearance in those plasmas. So the onset of GAMs in TJ-II should be explained by some non-linear

coupling of these modes. Reference [16] shows the possibility of a possible driving of GAMs by fast particle driven modes

3.3.- High frequency modes.

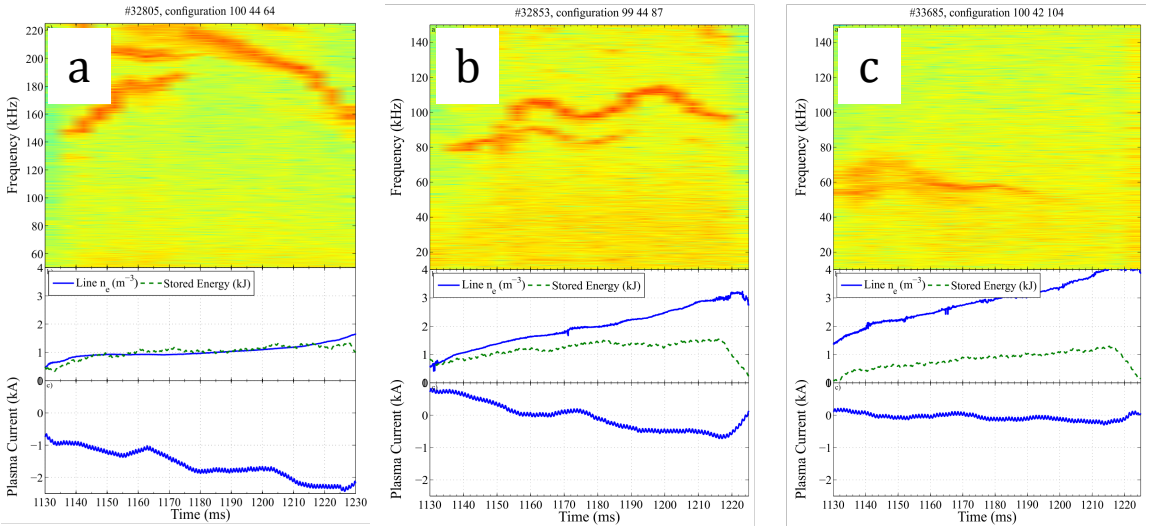

Figure 10. Turbulence spectra measured by Langmuir probes, together with the evolution of plasma current, density and storage energy, in three configurations: a) 100_44_64 (W=2.27); b) 99_44_87 (W=0.32%); c) 100_42_104 (W=-0.69%).

Despite of the fact that the vacuum rotational transform is very similar in all the cases, the mode structure changes drastically when decreasing the magnetic well, showing a non-monotonic behaviour of the amplitude, and a decrease of the typical frequencies. Figure 10 a, b, c) shows the onset of the Alfvén mode for three configurations with co-NBI, the first one with deep magnetic well, the second with an intermediate value and the third one presenting magnetic hill. The mode is of Alfvénic nature in the three cases (The mode spectrum in 4a that appears between 1135 and 1170 ms at freq. between 145 and 180 is an artefact due to aliasing and the frequency should be the mirror image). It is possible to detect in the three cases the frequency dependence on current and density given by Eq. (4).

The counter NBI heated plasmas show the same trend of decreasing frequencies when magnetic well decreases, but a larger variety of modes appear due to the different fast ion population.

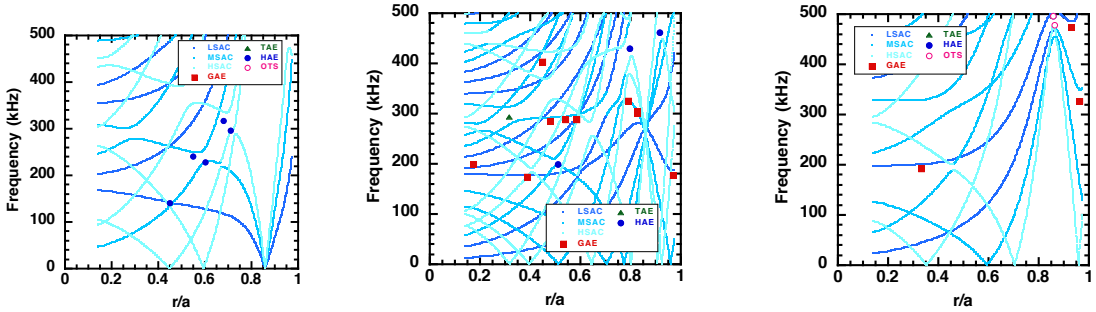

Figure 11: Calculations of the spectrum with STELLGAP for the configuration 100_44_64, for the families a) Nf=0, b) Nf=1, c) Nf= 2, showing the frequency and position of the possible modes.

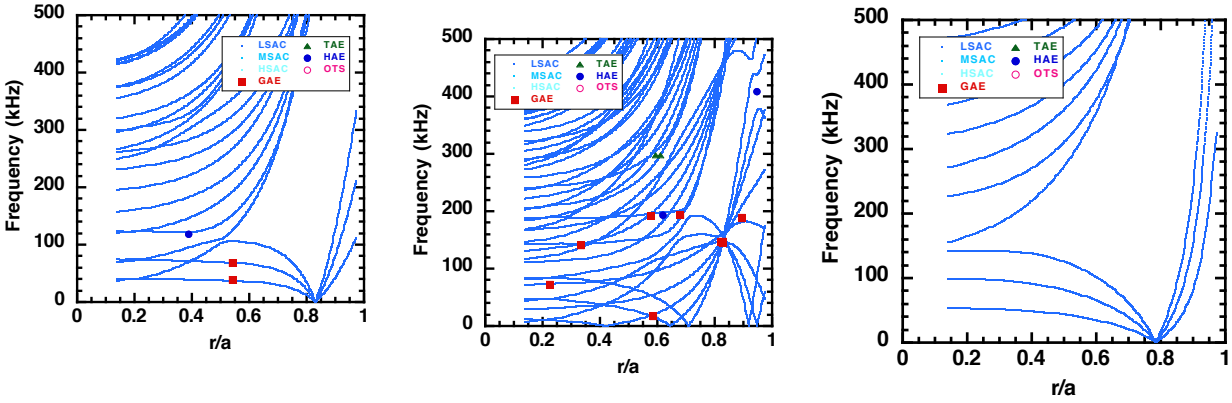

Figure 12

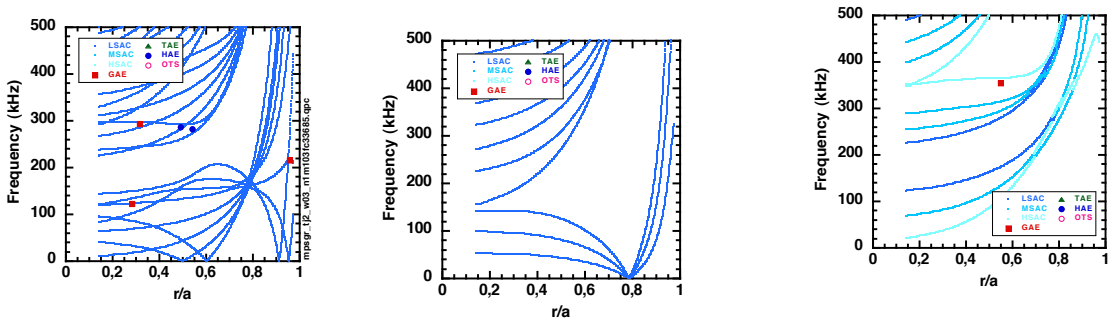

4.- comparison with simulations.

As it has been stated above, the frequency changes observed from one configuration to another must be attributed to the changes in the magnetic configuration, as it is shown by calculations performed with the codes STELLGAP and A3D[17], which can justify the strong frequency variation from one configuration to another one, as well as the spatial location.

We consider the experimental conditions of the cases shown in Figure 10, including the current and the density profiles. The current profile is assumed to be given by Spitzer. Figure 11a, b, c) shows the calculations performed with STELLGAP for the configuration 100_44_64, with magnetic well W=2.27 for three families of modes $N_f = 0, 1, 2$. The symbols in the figure mark the radial position and the frequency of the modes. The nature of the modes is also marked. These possible destabilised modes can be compared with the experimental results, regarding the frequency and position. We can then compare Figure 10a with Figure 11. We see that the possible modes that are destabilised are a HAE located at $\rho \approx 0.45$ of family N_f=0 (see figure 11a) or a GAE at $\rho \approx 0.4$ belonging to the family of family $N_f = 1$ (see figure 11b). These positions are in qualitative agreement with HIBP measurements.

In order to characterise the modes appearing in the configuration 99_44_87 (with magnetic well W=0.32%), we have a look to Figure 10b and 12, the mode that appears in the configuration could be a HAE whose maximum is located close to $\rho \approx 0.45$, belonging to the family $N_f = 0$ or it could be a GAE with maximum located close to $\rho \approx 0.3$ and belonging to the family $N_f = 1$. The position is in qualitative agreement with HIBP measurements, which show pretty wide modes.

Finally, the properties of the modes that appear in configuration 100_42_104 (with magnetic well W=-0.69%) can be explored considering Figures 10c and Figure 13. Considering the frequency that appears and the location of the mode measured by HIBP, we

see that the mode that appears could be a GAE at $\rho \approx 0.3$ of family $N_f = 1$. The calculated location is in qualitative agreement with HIBP measurements, but the calculated frequency is too high in comparison with the experimental results.

5.- Sumary and Conclusions

Previous studies of the effect of reducing magnetic well have shown a modest influence, if any, of magnetic well on global confinement. Nevertheless, the level of fluctuations detected by Langmuir probes strongly depends on the magnetic configuration and an increase of the level of electrostatic turbulence, detected by the Langmuir probes, happens for decreasing magnetic well.

The spectrum of wave vector, measured using Doppler reflectometer, does not depend on magnetic well, showing the same role of the scales in the configurations with different magnetic well scan.

The typical frequencies of the Alfvén modes that appear in the co-NBI heating tend to decrease with the magnetic well, as does their radial position. Calculations with STELLGAP have shown a reasonable agreement between the measurements and the estimatins, with the exception of the calculated frequency of the mode that appears in the configuration with smaller magnetic hill, which happens to be too high.

Finally, a GAM is found at intermediate frequencies, despite of the strong damping that the calculations predict for TJ-II.

These findings show that the effect of magnetic well is very limited in the general confinement properties, although the changes in magnetic turbulence could affect the fast ion transport.

Acknowledgements

This work has been carried out within the framework of the EUROfusion Consortium and has received funding from the Euratom research and training programme 2014-2018 under grant agreement No 633053. The views and opinions expressed herein do not necessarily reflect those of the European Commission.

[1] A. A. Subbotin et al. Nucl. Fusion 46 (2006) 921
[2] F. Castejón et al. Plasma Phys. Control. Fusion 55 (2013) 014003
[3] Referencia Mercier
[4] A. Varias et al. Nuclear Fusion, 1990

[5] Mikhailov, Shafranov,...
[6] REf. TJ-II
[7] A. M. Aguilera et al. "Magnetic well scan and confinement in the TJ-II stellarator". Submitted to Nucl. Fusion F. Castejón et al. Proc. of the 25th IAEA-FEC. Paper EX/P4-45. St. Petersburg, Russia, 2014.

[8] Ref. VMEC
[9] Ref. HIBP
[10] Reference Doppler
[11] A. Melnikov et al. Nucl. Fusion 54 (2014) 123002 (11pp)
[12] M. Aurelio.
[13] F. Castejón NF 2004
[14] C. R. Cook and C. C. Hegna. Physics of Plasmas 22, 042517 (2015)
[15] E. Sánchez. PPCF 2013
[16] T. Estrada et al. Nucl. Fusion xx (2015) xx
[17] D. A. Spong, R. Sanchez, A. Weller. Phys. Plasmas 10 (2003) 3217